Chinese Physics Letters

LETTER

Hall Coefficient Sign Reversal Driven by Orbital-Selective Oxygen-Vacancy Scattering in Nickelate Films

Cite as: Jian-Jian Miao *et al*. 2026 *Chin. Phys. Lett.* **43** 090706

DOI CSTR

Recommended Articles

Spin-Excitation Response to Oxygen Deficiency in $La_3Ni_2O_{7-\delta}$ Thin Films

Hengyang Zhong *et al*.
Chin. Phys. Lett. **43**, 060717 (2026)

Pressure-Driven Electronic Reconstruction and Anomalous Hall Transport Evolution in Monoclinic $FeNbTe_2$

Pengyu Su, Zhaoyu Zhu, Jingyi He, Jing Wang, Weiwei Wang, Chenchao Xu, Haiyang Yang, and Jie Wu
Chin. Phys. Lett. **43**, 070705 (2026)

Detecting Pairing Symmetry of Bilayer Nickelates Using Electronic Raman Scattering

Jun Zhan, Matías Bejas, Andreas P. Schnyder, Andrés Greco, Xianxin Wu, and Jiangping Hu
Chin. Phys. Lett. **43**, 020706 (2026)

Layer-Valley Hall Effect under Inversion and Time-Reversal Symmetries

Jiaojiao Zhao, Gui-Bin Liu, Peng Chen, Yugui Yao, Guangyu Zhang, and Luojun Du
Chin. Phys. Lett. **41**, (2024)

Electric-Field Control of Spin and Orbital Hall Effects in a Nodal-Ring Heterostructure Independent of Spin-Orbit Coupling

Zhikuan Wang, Wei Tan, Jianfeng Wang, Zeyu Jiang, and Bing Huang
Chin. Phys. Lett. **43**, 040705 (2026)

Granular Superconductivity in $La_2PrNi_2O_{7-\delta}$ Thin Films

Ziao Han, Lifen Xiang, Xingjiang Zhou, and Zhihai Zhu
Chin. Phys. Lett. , (2026)

A series journal of Chinese Physical Society distributed by IOP Publishing

Chinese Physics Letters

Chin. Phys. Lett. **43** 090706 (2026)

LETTER

DOI: 10.1088/0256-307X/43/9/090706
CSTR: 32039.14.0256-307X.43.9.090706

Hall Coefficient Sign Reversal Driven by Orbital-Selective Oxygen-Vacancy Scattering in Nickelate Films

Jian-Jian Miao(苗舰舰)[1,*], Yue Liu(刘越)[2], Yue Zhao(赵越)[2], Yichen Hua(华翌辰)[1,2], Changming Yue(岳长明)[2,3,*], and Wei-Qiang Chen(陈伟强)[2,4,1,*]

[1]Quantum Science Center of Guangdong-Hong Kong-Macao Greater Bay Area, Shenzhen 518045, China
[2]State Key Laboratory of Quantum Functional Materials, Department of Physics, and Guangdong Basic Research Center of Excellence for Quantum Science, Southern University of Science and Technology, Shenzhen 518055, China
[3]Guangdong Provincial Key Laboratory of Advanced Thermoelectric Materials and Device Physics, Southern University of Science and Technology, Shenzhen 518055, China
[4]Shenzhen Key Laboratory of Advanced Quantum Functional Materials and Devices, Southern University of Science and Technology, Shenzhen 518055, China

[*]Corresponding authors. Email: miaojianjian@quantumsc.cn; yuecm@sustech.edu.cn; chenwq@sustech.edu.cn

Hall measurements in superconducting bilayer nickelate films show sign reversals that cannot be explained by rigid-band electron doping alone. We combine a DFT+CDMFT-derived correlated multi-orbital quasiparticle model with a *T*-matrix treatment of oxygen-vacancy scattering in a semiclassical Boltzmann transport framework. We find that multiband compensation is insufficient by itself: in-plane vacancies selectively suppress the transport channel dominated by the $d_{x^2-y^2}$ orbital and drive R_H through zero, whereas inner-apical vacancies make R_H more negative. These results identify pocket-resolved and orbital-selective oxygen-vacancy scattering as the microscopic origin of the Hall coefficient sign reversal and provide a framework for oxygen-stoichiometry-dependent transport in nickelate films.

Nickelate superconductivity has rapidly emerged as an important frontier in correlated quantum materials, beginning with infinite-layer $Nd_{1-x}Sr_xNiO_2$ films [1] and then extending to Ruddlesden–Popper bilayer $La_3Ni_2O_7$ under high pressure [2]. More recently, ambient-pressure superconductivity in compressively strained bilayer films [3,4] has enabled structural, transport, optical, and spectroscopic probes that are difficult under pressure. Experiments now cover film and bulk transport [5–11], oxygen stoichiometry and defects [12–14], ARPES, STM, XAS/RIXS, and optical spectroscopy [15–21], and NMR/NQR, μSR, and neutron probes of density-wave order [22–28]. In parallel, theory has addressed multiorbital electronic structures, correlations, and pairing from weak-coupling to strong-coupling approaches [29–49]; recent reviews summarize the broader landscape [50–54].

Hall transport has long been central to high-temperature superconductivity: in cuprates, R_H, the Hall number, and the Hall angle track carrier evolution [55–59], reveal Fermi-surface reconstruction [60–62], and diagnose unconventional scattering [63–65]. In nickelate films, temperature-, field-, pressure-, and thickness-dependent measurements reveal positive, near-zero, and negative R_H values and sign changes [3,4,7,8,10,66]. Because film quality, doping, oxygen stoichiometry, disorder, and inhomogeneity vary among samples, a unified microscopic interpretation of R_H remains unsettled. A recent half-dome experiment tracked R_H across oxygen-rich, stoichiometric, and oxygen-deficient regimes and observed a Hall coefficient sign reversal upon introducing oxygen vacancies [67]. Although such sign reversals have been broadly attributed to multiband effects, what selects the competing pocket and orbital transport channels has not been clarified microscopically.

In this Letter, we provide a microscopic theory for the Hall coefficient sign reversal in superconducting bilayer nickelate films. Starting from a correlated multi-orbital quasiparticle model, we incorporate a T-matrix treatment of elastic oxygen-vacancy scattering into a semiclassical Boltzmann transport framework. This framework separates rigid-band doping from vacancy-scattering-induced changes in pocket-resolved and orbital-selective transport relaxation times. We show that multiband compensation alone is insufficient: in-plane vacancies select the pocket and orbital channels by suppressing the $d_{x^2-y^2}$ orbital contribution more strongly than the d_{z^2} contribution, thereby driving R_H through zero. Our results provide a microscopic interpretation of the experimentally observed evolution of R_H with oxygen stoichiometry and identify oxygen-vacancy scattering as a key control parameter for normal-state transport in bilayer nickelate films.

Quasiparticle Model

We start from the correlated multi-orbital model of the bilayer nickelate film obtained from DFT+CDMFT [68], which reproduces the ARPES Fermiology of superconducting nickelate heterostructures [16]. The low-energy electronic structure is captured by the four orbitals (A_x, A_z, B_x, B_z), where A/B labels the two NiO_2 layers and $x/z \equiv d_{x^2-y^2}/d_{z^2}$. Introducing the (anti-)bonding basis (z_+, x_+, x_-, z_-), with $z_\pm = (A_z \pm B_z)/\sqrt{2}$ and $x_\pm = (A_x \pm B_x)/\sqrt{2}$, the quasiparticle Hamiltonian is $H_{QP} = \sum_{\boldsymbol{k},\sigma} \boldsymbol{d}^\dagger_{\boldsymbol{k}\sigma} H_{QP}(\boldsymbol{k}) \boldsymbol{d}_{\boldsymbol{k}\sigma}$, where $\boldsymbol{k}$ is the two-dimensional momentum, σ is the spin index, and $\boldsymbol{d}_{\boldsymbol{k}\sigma} = (d_{\boldsymbol{k}z_+\sigma}, d_{\boldsymbol{k}x_+\sigma}, d_{\boldsymbol{k}x_-\sigma}, d_{\boldsymbol{k}z_-\sigma})^T$. The quasiparticle Hamiltonian matrix reads

$$H_{QP}(\boldsymbol{k}) = \hat{Z}^{1/2}[U^\dagger H_{DFT}(\boldsymbol{k}) U - \mu \hat{I} + \mathrm{Re}\hat{\Sigma}(0)]\hat{Z}^{1/2}, \tag{1}$$

where $H_{DFT}(\boldsymbol{k})$ is the DFT-derived tight-binding Hamiltonian in the layer-orbital basis, U is the unitary matrix that transforms the layer-orbital basis to the (anti-)bonding basis, μ is the chemical potential, $\hat{I}$ is the identity matrix, and $\mathrm{Re}\hat{\Sigma}(0)$ is the real part of the zero-frequency self-energy. The quasiparticle-weight matrix $\hat{Z}$, which plays an important role in the Hall-effect analysis, is included explicitly. In the DMFT calculation, both $\hat{\Sigma}$ and $\hat{Z}$ are diagonal in the (anti-)bonding basis; details are given in the Supplemental Material (SM). The band structure is obtained by diagonalizing Eq. (1), $H_{QP}(\boldsymbol{k})\phi_{m\boldsymbol{k}} = E_{m\boldsymbol{k}}\phi_{m\boldsymbol{k}}$, where m is the band index, $E_{m\boldsymbol{k}}$ is the quasiparticle dispersion measured from the Fermi level, and $\phi_{m\boldsymbol{k}}$ is the eigenstate in the (anti-)bonding basis. The resulting quasiparticle Fermi surface, shown in

Received 21 July 2026; accepted 18 August 2026; published 22 September 2026
© 2026 Chinese Physical Society and IOP Publishing Ltd. All rights, including for text and data mining, AI training, and similar technologies, are reserved.

Check for updates

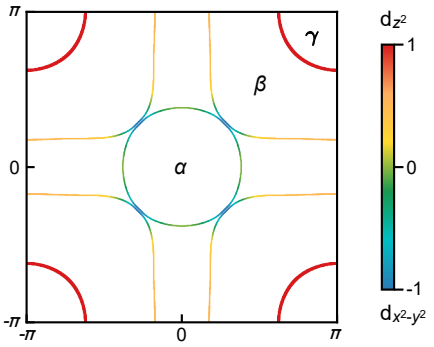

Fig. 1. Quasiparticle Fermi surface colored by the relative $d_{x^2-y^2}$ orbital weight $P^x = 1-2W^x$.

Fig. 1, consists of three pockets α, β, and γ. We denote the orbital weight as $W^r_{mk} = |\phi_{mk,r_+}|^2 + |\phi_{mk,r_-}|^2$, $r = x, z$, and define the relative $d_{x^2-y^2}$ orbital weight as $P^x_{mk} = 1-2W^x_{mk}$. Then the colored quasiparticle Fermi surface in Fig. 1 shows that the α and γ pockets are predominantly derived from $d_{x^2-y^2}$ and d_{z^2} orbitals, respectively, whereas the β pocket has mixed orbital character.

Weak-Field Hall Coefficient

The key transport observable addressed here is the Hall coefficient of nickelate films. The semiclassical treatment is applicable to the normal-state weak-field regime, where quasiparticles are well defined ($k_F\ell \gg 1$) and $\omega_c\tau \ll 1$; superconducting fluctuations, localization, and incoherent transport near the insulating limit lie outside its scope. We label the three pocket contours by C_u, with $u = \alpha, \beta, \gamma$, and define the band velocity and mean-free-path vector as $\boldsymbol{v}^u_{\boldsymbol{k}} = \hbar^{-1}\nabla_{\boldsymbol{k}}E_{u\boldsymbol{k}}$ and $\boldsymbol{\ell}^u_{\boldsymbol{k}} = \tau^u_{\boldsymbol{k}}\boldsymbol{v}^u_{\boldsymbol{k}}$, respectively. Here $\tau^u_{\boldsymbol{k}}$ is the transport relaxation time. The longitudinal conductivity is written as a line integral over the pocket contours,

$$\sigma_{aa} = \sum_u \frac{g_s e^2}{(2\pi)^2\hbar}\oint_{C_u}\frac{\mathrm{d}k}{|\boldsymbol{v}^u_{\boldsymbol{k}}|}\tau^u_{\boldsymbol{k}}(\boldsymbol{v}^u_{\boldsymbol{k}}\cdot\hat{\boldsymbol{e}}_a)^2, \tag{2}$$

with $a = x, y$ and spin degeneracy $g_s = 2$. From Ong's geometrical interpretation, the weak-field Hall conductivity is related to the signed area A^u_ℓ swept out by $\boldsymbol{\ell}^u$ in mean-free-path space [69],

$$\frac{\sigma_{xy}}{B} = \sum_u \frac{\sigma^u_{xy}}{B} = \sum_u \frac{g_s e^3}{h^2}A^u_\ell, \quad A^u_\ell = \frac{1}{2}\oint_{C_u}(\ell^u_x \mathrm{d}\ell^u_y - \ell^u_y \mathrm{d}\ell^u_x). \tag{3}$$

Owing to the separability of the pocket contours, we define the *pocket-resolved* contributions to the Hall coefficient as

$$R_H = \sum_u R^u_H, \quad R^u_H = \frac{\sigma^u_{xy}/B}{\sigma_{xx}\sigma_{yy}}, \tag{4}$$

where $R_H = \rho_{yx}/B \simeq \sigma_{xy}/(B\sigma_{xx}\sigma_{yy})$ has been used. The derivation of the Hall coefficient formula is given in the SM. Within this geometrical picture, the sign of R_H is determined by the total signed area $\sum_u A^u_\ell$, so that the sign reversal occurs when

$$\sum_u A^u_\ell = 0. \tag{5}$$

Since the three pockets carry distinct orbital characters, this compensation among pocket-resolved contributions also encodes the competition between orbital-selective contributions.

Vacancy-Free Limit

We roughly estimate the Hall coefficient without oxygen vacancies as the baseline for the subsequent calculations. In this vacancy-free limit, we assume a constant transport relaxation time, $\tau^u_{\boldsymbol{k}} = \tau_0$. Then, $\sigma_{aa} \propto \tau_0$ and $\sigma_{xy} \propto \tau_0^2$, so that $R_H \propto \sigma_{xy}/(\sigma_{xx}\sigma_{yy})$ is independent of τ_0. Under this assumption, we obtain $R_H = -0.2817\times10^{-3}$ cm^3/C, which has the same sign and order of magnitude as the experimental value reported for optimized, near-stoichiometric bilayer-nickelate films [67]. This justifies using the quasiparticle Fermi surface as a reasonable starting point before introducing oxygen vacancies. Although the Hall coefficient is not directly orbital resolved, we introduce the pocket-averaged orbital weights and define the *orbital-selective* contributions to the Hall coefficient as

$$\overline{W}^r_u = \frac{\oint_{C_u}\mathrm{d}k\, W^r_{uk}/|\boldsymbol{v}^u_{\boldsymbol{k}}|}{\oint_{C_u}\mathrm{d}k/|\boldsymbol{v}^u_{\boldsymbol{k}}|}, \quad R^r_H = \sum_u \overline{W}^r_u R^u_H. \tag{6}$$

The pocket-resolved and orbital-selective contributions to the vacancy-free Hall coefficient are listed in Table 1. We note that the γ pocket contributes only weakly to R_H. In Ong's geometrical interpretation, this weak contribution reflects the small mean-free-path contour formed by the weakly dispersive γ pocket owing to its small Fermi velocities. Therefore, in the vacancy-free limit, the orbital selectivity primarily arises from the compensation between the α and β pockets.

Table 1. Pocket-resolved and orbital-selective contributions to the vacancy-free Hall coefficient. Values are in units of 10^{-3} cm^3/C. The numerical calculation details are given in the SM.

Pocket	R^u_H	Orbital	R^r_H
α	−1.2835	$d_{x^2-y^2}$	−0.5140
β	+0.9985	d_{z^2}	+0.2323
γ	+0.0033		

Table 2. Pocket-resolved and orbital-selective contributions to the rigid-band Hall coefficient at $n_{vac} = 0.1$. Values are in units of 10^{-3} cm^3/C.

Pocket	R^u_H	Orbital	R^r_H
α	−1.3326	$d_{x^2-y^2}$	−0.5692
β	+1.0736	d_{z^2}	+0.3107
γ	+0.0005		

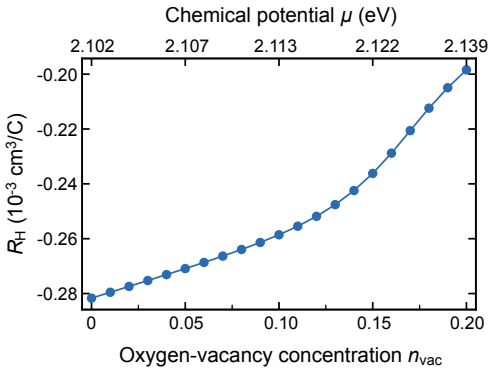

Fig. 2. Rigid-band R_H as a function of n_{vac} and μ.

Oxygen-Vacancy Doping Effect

We now turn to the effect of oxygen vacancies on the Hall coefficient. Physically, their main role can be analyzed from two perspectives: the doping effect associated with oxygen removal and the impurity-scattering effect introduced by the oxygen-vacancy potential. To clarify the key ingredients for the Hall coefficient sign reversal, we consider these two effects separately. Theoretically, as a leading-order approximation, we model the doping effect within a rigid-band approximation by tuning the chemical potential of the quasiparticle band structure. Figure 2 plots rigid-band R_H as a function of the oxygen-vacancy concentration n_{vac} and the corresponding chemical potential μ. Comparing the results in Tables 1 and 2, the increase in

the positive β-pocket contribution outweighs the enhanced negative α-pocket contribution, making the rigid-band $R_{\rm H}$ less negative. The orbital-selective contributions evolve in the same way as the α- and β-pocket contributions. However, rigid-band $R_{\rm H}$ remains negative over the range considered, suggesting that doping alone does not account for a Hall coefficient sign reversal.

Orbital-Selective Scattering Potential

To study the impurity-scattering effect, we construct the single-vacancy scattering potential from first-principles DFT calculations. In the dilute-vacancy limit, interactions between different oxygen vacancies are neglected, allowing inner-apical and in-plane vacancies to be treated separately. The vacancy-induced tight-binding parameter changes are obtained by applying the same DFT-Wannier workflow to the vacancy-free and relaxed single-vacancy structures; computational details are given in the SM. Importantly, this procedure yields a microscopic tight-binding model of the local vacancy potential rather than phenomenological impurity parameters. For an inner-apical vacancy, the largest changes are the neighboring d_{z^2} orbital onsite energy, $\Delta\epsilon_z = -1.12$ eV, and the strong reduction of the interlayer d_{z^2} hopping, $\Delta t_\perp^z = +0.45$ eV. By contrast, an in-plane vacancy mainly affects the adjacent $d_{x^2-y^2}$ sector, with $\Delta\epsilon_x = -1.34$ eV, together with sizable local changes in $d_{x^2-y^2}$ hopping and $d_{x^2-y^2}$-d_{z^2} hybridization of order 0.2–0.3 eV. This strong orbital contrast originates from the vacancy-induced distortion of the oxygen octahedra, which modifies the local crystal-field environment, and provides the microscopic basis for orbital-selective oxygen-vacancy scattering.

Hall Coefficient Sign Reversal

We next examine the impurity-scattering effects on the Hall coefficient from *inner-apical* and *in-plane* oxygen vacancies. Combining the T-matrix with the semiclassical Boltzmann transport framework, the scalar relaxation-time approximation gives

$$\frac{1}{\tau_{m\boldsymbol{k}}} = \frac{2\pi}{\hbar} n_{\rm vac} \sum_{m'} \int_{\rm BZ} \frac{{\rm d}^2 k'}{(2\pi)^2} |T^R_{m'm}|^2 (1 - \hat{\boldsymbol{v}}_{m\boldsymbol{k}} \cdot \hat{\boldsymbol{v}}_{m'\boldsymbol{k}'}) \times \delta(E_{m\boldsymbol{k}} - E_{m'\boldsymbol{k}'}), \tag{7}$$

where $\tau_{m\boldsymbol{k}}$ is the transport relaxation time of the quasiparticle state $|m\boldsymbol{k}\rangle$ due to oxygen-vacancy elastic scattering, $\hat{\boldsymbol{v}}_{m\boldsymbol{k}} = \boldsymbol{v}_{m\boldsymbol{k}}/|\boldsymbol{v}_{m\boldsymbol{k}}|$, and $T^R_{m'm} \equiv T^R_{m'm}(\boldsymbol{k}', \boldsymbol{k}; E_{m\boldsymbol{k}})$ is the retarded T-matrix in the band basis generated by the oxygen-vacancy scattering potential. Here δ denotes the Dirac delta function ensuring elastic energy conservation. The derivation is given in the SM. Since the total transport relaxation time is now band- and momentum-dependent, the Hall coefficient also depends on the vacancy-free transport relaxation time τ_0. A calibration from the semiclassical Boltzmann transport framework to the longitudinal resistivity reported in Ref. [4] gives a nominal $\tau_0 \simeq 5.8$ fs. In consideration of other scattering channels such as inelastic scattering and incoherent transport, the actual vacancy-free transport relaxation time is usually larger by one to two orders of magnitude. Therefore, in the following calculations we take $\tau_0 = 50$ fs. For a distribution with $a\%$ inner-apical and $b\%$ in-plane oxygen vacancies, the total transport relaxation time is obtained from Matthiessen's rule,

$$\frac{1}{\tau^{\rm tot}_{m\boldsymbol{k}}} = \frac{1}{\tau_0} + a\% \frac{1}{\tau^{\rm ap}_{m\boldsymbol{k}}} + b\% \frac{1}{\tau^{\rm pl}_{m\boldsymbol{k}}}, \tag{8}$$

where $a + b = 100$, and $\tau^{\rm ap}_{m\boldsymbol{k}}$ and $\tau^{\rm pl}_{m\boldsymbol{k}}$ are the transport relaxation times induced by inner-apical and in-plane oxygen vacancies, respectively. Figure 3 shows three robust trends: inner-apical vacancies make $R_{\rm H}$ more negative without a sign reversal, in-plane vacancies drive $R_{\rm H}$ through zero, and mixed distributions reverse sign more readily as the in-plane-vacancy fraction increases. Thus, the multiband structure supplies competing Hall channels, but in-plane oxygen-vacancy scattering selects them and produces the sign reversal. The sign-change

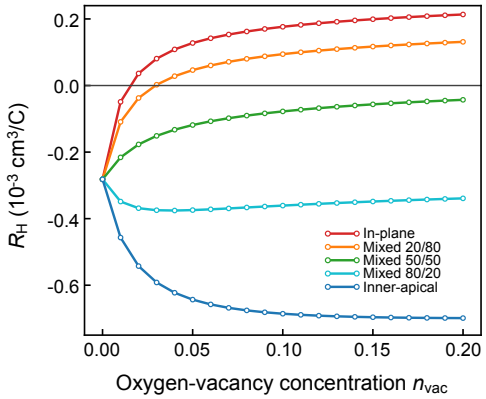

Fig. 3. $R_{\rm H}$ as a function of $n_{\rm vac}$ for five oxygen-vacancy distributions, with $\tau_0 = 50$ fs. A mixed distribution a/b denotes $a\%$ inner-apical and $b\%$ in-plane oxygen vacancies.

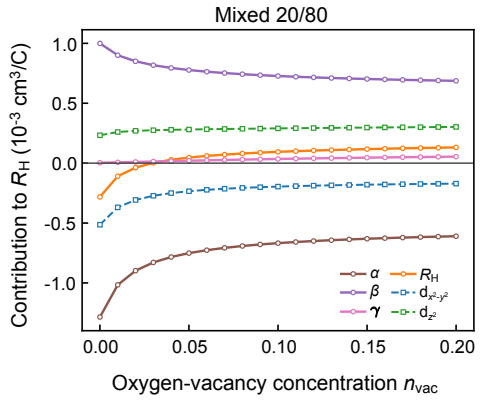

Fig. 4. Pocket-resolved (solid lines) and orbital-selective (dashed lines) contributions to $R_{\rm H}$ for the mixed 20/80 distribution, with $\tau_0 = 50$ fs.

concentration $n^*_{\rm vac}$ defined by $R_{\rm H}(n^*_{\rm vac}) = 0$ shifts only quantitatively when τ_0 is varied from 10 to 500 fs (see SM), and the saturation at large $n_{\rm vac}$ follows from $\sigma_{aa} \propto 1/n_{\rm vac}$ and $\sigma_{xy} \propto 1/n^2_{\rm vac}$ once vacancy scattering dominates Eq. (8). Figure 4 resolves the mechanism for the mixed 20/80 distribution: oxygen-vacancy scattering suppresses both α and β pocket contributions, but the α contribution is reduced more strongly, driving the total Hall coefficient positive. The apparent increase of the γ contribution originates mainly from the reduced longitudinal conductivities in the denominator of $R^\gamma_{\rm H}$, rather than from an enhanced pocket-resolved Hall conductivity. In orbital space, the $d_{x^2-y^2}$ contribution decreases markedly while the d_{z^2} contribution remains nearly unchanged, establishing the orbital-selective origin of the sign reversal.

Discussion

Our results establish oxygen vacancies as an active microscopic control of Hall transport in bilayer nickelate films, rather than a passive source of electron doping. The multiband Fermi surface provides competing Hall channels, but the sign reversal is selected by how oxygen vacancies scatter distinct pocket and orbital sectors. In particular, in-plane oxygen vacancies suppress the $d_{x^2-y^2}$ orbital contribution and drive $R_{\rm H}$ through zero, whereas inner-apical vacancies enhance the negative Hall response. This orbital and site selectivity provides a microscopic interpretation for the broad spread of positive, nearly zero, and negative Hall coefficients reported in films with different oxygen stoichiometry, vacancy distributions, and disorder. Existing experiments on Sr-doped bilayer nickelate films find that oxygen vacancies predominantly occupy in-plane rather than apical sites, further supporting this theoretical picture [7]. This site-selective prediction is directly testable by correlating Hall measurements with site-resolved

characterization of oxygen vacancies: at comparable total n_{vac}, increasing the in-plane-vacancy fraction should drive R_H toward and through zero, whereas increasing the inner-apical-vacancy fraction should make R_H more negative.

This mechanism also places the nickelate Hall sign reversal in a different category from the more familiar routes discussed in cuprates. In high-temperature superconductors, anomalous Hall responses have been interpreted through marginal-Fermi-liquid and small-angle-scattering phenomenology [70,71], strongly correlated theories based on doped Mott insulators or Hubbard/t–J models [72,73], and Fermi-surface reconstruction by stripe, density-wave, or antiferromagnetic order [74–77]. For the nickelate films considered here, however, no pronounced resistive anomaly is observed near the Hall sign reversal that would signal such an ordered-state reconstruction. The present work therefore identifies a disorder-enabled, orbital-selective route to Hall sign reversal in a correlated multiorbital metal. A more complete description of the temperature-, field-, pressure-, and thickness-dependent Hall response may require more sophisticated treatments, such as current vertex corrections in the presence of antiferromagnetic fluctuations [78,79], which go beyond the semiclassical Boltzmann transport framework used in this Letter. More broadly, it shows that Hall measurements, when combined with structural probes of oxygen defects, can diagnose the vacancy landscape and orbital-selective scattering in the normal state. Consistently, oxygen-content studies of bilayer nickelate films find that, as oxygen defects increase and the system approaches the insulating regime, the resistance can be well fitted by Mott variable-range hopping behavior, indicating the pronounced disorder effect induced by oxygen defects [80].

Acknowledgments

We thank Heng Wang and Kun Jiang for helpful discussions. This work was supported by the National Key Research and Development Program of China (Grant No. 2022YFA1403702), the National Natural Science Foundation of China (Grant Nos. 12404171 and 12334002), the Guangdong Project (Grant No. 2024QN11X176), the Guangdong Provincial Quantum Science Strategic Initiative (Grant No. SZZX 2401001), the Science, Technology and Innovation Commission of Shenzhen Municipality (Grant No. ZDSYS20190902092905285), and the Center for Computational Science and Engineering at Southern University of Science and Technology. Changming Yue acknowledges support from the Guangdong Provincial Quantum Science Strategic Initiative (Grant Nos. GDZX2401004 and GDZX2501001) and the National Natural Science Foundation of China (Grant No. 12474231).

References

[1] Li D, Lee K, Wang B Y, Osada M, Crossley S, Lee H R, Cui Y, Hikita Y, and Hwang H Y 2019 *Nature* **572** 624
[2] Sun H, Huo M, Hu X, Li J, Liu Z, Han Y, Tang L, Mao Z, Yang P, Wang B, Cheng J, Yao D X, Zhang G M, and Wang M 2023 *Nature* **621** 493
[3] Ko E K, Yu Y, Liu Y, Bhatt L, Li J, Thampy V, Kuo C T, Wang B Y, Lee Y, Lee K, Lee J S, Goodge B H, Muller D A, and Hwang H Y 2025 *Nature* **638** 935
[4] Zhou G, Lv W, Wang H, Nie Z, Chen Y, Li Y, Huang H, Chen W Q, Sun Y J, Xue Q K, and Chen Z 2025 *Nature* **640** 641
[5] Wang N, Wang G, Shen X, Hou J, Luo J, Ma X, Yang H, Shi L, Dou J, Feng J, Yang J, Shi Y, Ren Z, Ma H, Yang P, Liu Z, Liu Y, Zhang H, Dong X, Wang Y, Jiang K, Hu J, Nagasaki S, Kitagawa K, Calder S, Yan J, Sun J, Wang B, Zhou R, Uwatoko Y, and Cheng J 2024 *Nature* **634** 579
[6] Zhang Y, Su D, Huang Y, Shan Z, Sun H, Huo M, Ye K, Zhang J, Yang Z, Xu Y, Su Y, Li R, Smidman M, Wang M, Jiao L, and Yuan H 2024 *Nat. Phys.* **20** 1269
[7] Hao B, Wang M, Sun W, Yang Y, Mao Z, Yan S, Sun H, Zhang H, Han L, Gu Z, Zhou J, Ji D, and Nie Y 2025 *Nat. Mater.* **24** 1756
[8] Liu Y, Ko E K, Tarn Y, Bhatt L, Li J, Thampy V, Goodge B H, Muller D A, Raghu S, Yu Y, and Hwang H Y 2025 *Nat. Mater.* **24** 1221
[9] Wang M, Sun H, Huo M, Hu X, Li J, Liu Z, Han Y, Tang L, Mao Z, Yang P, Cheng J, Yao D X, and Zhang G M 2026 *Phys. Rev. Lett.* **136** 066002
[10] Li Q, Sun J, Boetzel S, Ou M, Xiang Z N, Lechermann F, Wang B, Wang Y, Zhang Y J, Cheng J, Eremin I M, and Wen H H 2026 *Nat. Commun.* **17** 3276
[11] Nie Z, Li Y, Lv W, Xu L, Jiang Z, Fu P, Zhou G, Song W, Chen Y, Wang H, Huang H, Lin J, Jia J F, Shen D, Li P, Xue Q K, and Chen Z 2026 *Nature* **652** 628
[12] Dong Z, Huo M, Li J, Li J, Li P, Sun H, Lu Y, Wang M, Wang Y, and Chen Z 2024 *Nature* **630** 847
[13] Dong Z, Wang G, Wang N, Dong W H, Gu L, Xu Y, Cheng J, Chen Z, and Wang Y 2025 *Nat. Mater.* **24** 1927
[14] Shi M, Peng D, Li Y, Yang S, Xing Z, Wang Y, Fan K, Li H, Wu R, Ge B, Zeng Z, Zeng Q, Ying J, Wu T, and Chen X 2025 *Nat. Commun.* **16** 9141
[15] Yang J, Sun H, Hu X, Xie Y, Miao T, Luo H, Chen H, Liang B, Zhu W, Qu G, Chen C Q, Huo M, Huang Y, Zhang S, Zhang F, Yang F, Wang Z, Peng Q, Mao H, Liu G, Xu Z, Qian T, Yao D X, Wang M, Zhao L, and Zhou X J 2024 *Nat. Commun.* **15** 4373
[16] Li P, Zhou G, Lv W, Li Y, Yue C, Huang H, Xu L, Shen J, Miao Y, Song W, Nie Z, Chen Y, Wang H, Chen W, Huang Y, Chen Z H, Qian T, Lin J, He J, Sun Y J, Chen Z, and Xue Q K 2025 *Natl. Sci. Rev.* **12** nwaf205
[17] Li Y, Xu L, Lv W, Nie Z, Wang Z, Miao Y, Shen J, Zhou G, Song W, Wang H, Huang H, He J, Jia J F, Li P, Xue Q K, and Chen Z 2026 arXiv: 2604.08430 [cond-mat.supr-con]
[18] Fan S, Ou M, Scholten M, Li Q, Shang Z, Wang Y, and Wen H H 2026 *Sci. Adv.* **12** eaeg2429
[19] Wang X, Chen Y, Ding C, Xu L, Miao J J, Zhou G, Chen Z, Sun Y J, Jia J F, and Xue Q K 2026 arXiv: 2605.14806 [cond-mat.supr-con]
[20] Chen X, Choi J, Jiang Z, Mei J, Jiang K, Li J, Agrestini S, Garcia-Fernandez M, Huang X, Sun H, Shen D, Wang M, Hu J, Lu Y, Zhou K J, and Feng D 2024 *Nat. Commun.* **15** 9597
[21] Meng Y, Yang Y, Sun H, Zhang S, Luo J, Chen L, Ma X, Wang M, Hong F, Wang X, and Yu X 2024 *Nat. Commun.* **15** 10408
[22] Zhao D, Zhou Y, Huo M, Wang Y, Nie L, Wang M, Wu T, and Chen X 2025 *Sci. Bull.* **70** 1239
[23] Luo J, Feng J, Wang G, Wang N, Dou J, Fang A, Yang J, Cheng J, Zheng G, and Zhou R 2025 *Chin. Phys. Lett.* **42** 067402
[24] Yashima M, Seto N, Oshita Y, Kakoi M, Sakurai H, Takano Y, and Mukuda H 2025 *J. Phys. Soc. Jpn.* **94** 054704
[25] Chen K, Liu X, Jiao J, Zou M, Jiang C, Li X, Luo Y, Wu Q, Zhang N, Guo Y, and Shu L 2024 *Phys. Rev. Lett.* **132** 256503
[26] Khasanov R, Hicken T J, Gawryluk D J, Sazgari V, Plokhikh I, Sorel L P, Bartkowiak M, Bötzel S, Lechermann F, Eremin I M, Luetkens H, and Guguchia Z 2025 *Nat. Phys.* **21** 430
[27] Plokhikh I, Hicken T J, Keller L, Pomjakushin V, Moody S H, Foury-Leylekian P, Krieger J J, Luetkens H, Guguchia Z, Khasanov R, and Gawryluk D J 2025 arXiv: 2503.05287 [cond-mat.supr-con]
[28] Chen L, Zhang E, Hao Y, Zhu Y, Cui B, Abernathy D L, Williams T J, Ikeda Y, Zhang H, Liu F, Wang W, Wang Q, and Zhao J 2026 arXiv: 2605.03448 [cond-mat.str-el]
[29] Lechermann F, Gondolf J, Bötzel S, and Eremin I M 2023 *Phys. Rev. B* **108** L201121
[30] Fan Z, Zhang J F, Zhan B, Lv D, Jiang X Y, Normand B, and Xiang T 2024 *Phys. Rev. B* **110** 024514
[31] Cao Y and Yang Y F 2024 *Phys. Rev. B* **109** L081105
[32] Gu Y H, Le C C, Yang Z S, Wu X X, and Hu J P 2025 *Phys. Rev. B* **111** 174506
[33] Zhang Y, Lin L F, Moreo A, Maier T A, and Dagotto E 2024 *Nat. Commun.* **15** 2470
[34] Sakakibara H, Kitamine N, Ochi M, and Kuroki K 2024 *Phys. Rev. Lett.* **132** 106002
[35] Heier G, Park K, and Savrasov S Y 2024 *Phys. Rev. B* **109** 104508
[36] Jiang K Y, Cao Y H, Yang Q G, Lu H Y, and Wang Q H 2025 *Phys. Rev. Lett.* **134** 076001
[37] Xia C, Liu H, Zhou S, and Chen H 2025 *Nat. Commun.* **16** 1054
[38] Xi W, Yu S L, and Li J X 2025 *Phys. Rev. B* **111** 104505
[39] Lu C, Pan Z, Yang F, and Wu C 2024 *Phys. Rev. Lett.* **132** 146002
[40] Yang H, Oh H, and Zhang Y H 2024 *Phys. Rev. B* **110** 104517
[41] Jiang K, Wang Z, and Zhang F C 2024 *Chin. Phys. Lett.* **41** 017402
[42] Jiang R, Hou J, Fan Z, Lang Z J, and Ku W 2024 *Phys. Rev. Lett.* **132**

126503
[43] Luo Z, Lv B, Wang M, Wu W, and Yao D X 2024 *npj Quantum Mater.* **9** 61
[44] Zhang J X, Zhang H K, You Y Z, and Weng Z Y 2024 *Phys. Rev. Lett.* **133** 126501
[45] Schlömer H, Schollwöck U, Grusdt F, and Bohrdt A 2024 *Commun. Phys.* **7** 366
[46] Wang Z, Zhang H J, Jiang K, and Zhang F C 2025 *Natl. Sci. Rev.* **12** nwaf353
[47] Lange H, Homeier L, Demler E, Schollwöck U, Bohrdt A, and Grusdt F 2024 *Phys. Rev. B* **109** 045127
[48] Qu X Z, Qu D W, Chen J, Wu C, Yang F, Li W, and Su G 2024 *Phys. Rev. Lett.* **132** 036502
[49] Wang Z, Jiang K, Zhang F C, and Jin H K 2026 arXiv: 2604.08319 [cond-mat.str-el]
[50] Nomura Y and Arita R 2022 *Rep. Prog. Phys.* **85** 052501
[51] Wang M, Wen H H, Wu T, Yao D X, and Xiang T 2024 *Chin. Phys. Lett.* **41** 077402
[52] Puphal P, Schäfer T, Keimer B, and Hepting M 2026 *Nat. Rev. Phys.* **8** 70
[53] Wang Y, Jiang K, Ying J, Wu T, Cheng J, Hu J, and Chen X 2025 *Natl. Sci. Rev.* **12** nwaf373
[54] Miao J and Chen W 2026 *Acta Phys. Sin.* **75** 070701 (in Chinese)
[55] Ong N P, Wang Z Z, Hagen S J, Jing T W, Clayhold J A, and Horvath J 1987 *Phys. Rev. B* **35** 8807
[56] Hwang H Y, Batlogg B, Takagi H, Kao H L, Kwo J, Cava R J, Krajewski J J, and Peck W F 1994 *Phys. Rev. Lett.* **72** 2636
[57] Ando Y, Segawa K, Komiya S, and Lavrov A N 2004 *Phys. Rev. Lett.* **92** 197001
[58] Balakirev F F, Betts J B, Migliori A, Ono S, Ando Y, and Boebinger G S 2003 *Nature* **424** 912
[59] Badoux S, Tabis W, Laliberté F, Grissonnanche G, Vignolle B, Vignolles D, Béard J, Bonn D A, Hardy W N, Liang R, Doiron-Leyraud N, Taillefer L, and Proust C 2016 *Nature* **531** 210
[60] Doiron-Leyraud N, Proust C, LeBoeuf D, Levallois J, Bonnemaison J B, Liang R, Bonn D A, Hardy W N, and Taillefer L 2007 *Nature* **447** 565
[61] LeBoeuf D, Doiron-Leyraud N, Levallois J, Daou R, Bonnemaison J B, Hussey N E, Balicas L, Ramshaw B J, Liang R, Bonn D A, Hardy W N, Adachi S, Proust C, and Taillefer L 2007 *Nature* **450** 533
[62] Laliberté F, Chang J, Doiron-Leyraud N, Hassinger E, Daou R, Rondeau M, Ramshaw B J, Liang R, Bonn D A, Hardy W N, Pyon S, Takayama T, Takagi H, Sheikin I, Malone L, Proust C, Behnia K, and Taillefer L 2011 *Nat. Commun.* **2** 432
[63] Chien T R, Wang Z Z, and Ong N P 1991 *Phys. Rev. Lett.* **67** 2088
[64] Anderson P W 1991 *Phys. Rev. Lett.* **67** 2092
[65] Harris J M, Yan Y F, Matl P, Ong N P, Anderson P W, Kimura T, and Kitazawa K 1995 *Phys. Rev. Lett.* **75** 1391
[66] Shi Y, Song C, Jia Y, Wang Y, Li Q, Chen Y, Yang Y, Fu J, Qin M, Song D, Chen Z, Yuan H, Xie Y, and Zhang M 2025 *Adv. Mater.* **38** e10394
[67] Liu Y, Wang B Y, Li J, Tarn Y, Bhatt L, Colletta M, Wu Y M, Kuo C T, Lee J S, Goodge B H, Muller D A, Shen Z X, Raghu S, Hwang H Y, and Yu Y 2026 arXiv: 2603.12196 [cond-mat.supr-con]
[68] Yue C, Miao J J, Huang H, Hua Y, Li P, Li Y, Zhou G, Lv W, Yang Q, Sun H, Sun Y J, Lin J, Xue Q K, Chen Z, and Chen W Q 2025 *Natl. Sci. Rev.* **12** nwaf253
[69] Ong N P 1991 *Phys. Rev. B* **43** 193
[70] Varma C M and Abrahams E 2001 *Phys. Rev. Lett.* **86** 4652
[71] Abrahams E and Varma C M 2003 *Phys. Rev. B* **68** 094502
[72] Ioffe L B, Kalmeyer V, and Wiegmann P B 1991 *Phys. Rev. B* **43** 1219
[73] Veberič D and Prelovšek P 2002 *Phys. Rev. B* **66** 020408
[74] Chakravarty S, Nayak C, Tewari S, and Yang X 2002 *Phys. Rev. Lett.* **89** 277003
[75] Lin J and Millis A J 2005 *Phys. Rev. B* **72** 214506
[76] Millis A J and Norman M R 2007 *Phys. Rev. B* **76** 220503
[77] Eberlein A, Metzner W, Sachdev S, and Yamase H 2016 *Phys. Rev. Lett.* **117** 187001
[78] Kanki K and Kontani H 1999 *J. Phys. Soc. Jpn.* **68** 1614
[79] Kontani H, Kanki K, and Ueda K 1999 *Phys. Rev. B* **59** 14723
[80] Miao Y, Luan R, Chen Y, Ou Z, Zhou G, Shen J, Wang H, Huang H, Wu X, Sun H, Feng Z, Yong X, Li Y, Li P, Xu L, Lv W, Nie Z, Yue C, Sun Y J, Chen W, Yuan H, Jia J F, Xue Q K, Chen Z, and He J 2025 arXiv: 2502.18068 [cond-mat.supr-con]